Phys Chem Minerals (2005) 32: 578–584
DOI 10.1007/s00269-005-0033-2

ORIGINAL PAPER

L. F. Lundegaard · E. Makovicky
T. Boffa-Ballaran · T. Balic-Zunic

Crystal structure and cation lone electron pair activity of Bi_2S_3 between 0 and 10 GPa

Received: 1 March 2005 / Accepted: 15 August 2005 / Published online: 15 November 2005

Abstract Crystal structure of Bi_2S_3 was refined at eight distinct hydrostatic pressures in the range 0–10 GPa using a CCD equipped 4-circle diffractometer and a diamond-anvil cell. Coefficients of the BM3 equation of state are as follows: zero-pressure volume 498.4(7) $Å^3$, bulk modulus K_0 36.6(15) GPa and its pressure derivative 6.4(5). The bulk of compression takes place in the structural space between Bi_4S_6 ribbons, where lone-electron pairs are accommodated. Eccentricity of Bi in its coordination polyhedra decreases in the process, with long Bi–S distances decreasing, whereas the opposing short Bi–S distances stay constant or even increase in length. All these phenomena are compatible with the movement of lone-electron pairs of Bi closer to the parent atom at increasing pressure.

Keywords Bismuthinite · High pressure · Lone electron pair · Equation of state

Introduction

Stibnite, Sb_2S_3, and bismuthinite, Bi_2S_3, have recently become an object of renewed studies as simple representatives of compounds with active lone electron pairs on cations. The structure of Sb_2S_3 at ambient conditions was originally determined by Hofmann (1933) and revised by Šćavničar (1960), Bayliss and Nowacki (1972) as well as by Łukaszewicz et al. (1997); that of Bi_2S_3 by Kupčik and Veselá-Nováková (1970). They were re-refined by Lundegaard et al. (2003) and Kyono and Kimata (2004).

Low-temperature structure refinements on Sb_2S_3 were made by Kyono et al. (2002) and by Lundegaard (2003) whereas the high/low temperature transformation of this compound has been repeatedly approached by diverse physical methods and hotly discussed since the first paper of Rinkevichius and Mikalkevichius (1967) on the pyroelectric effect. The latest contributions, with diametrically opposing points of view, have been published by Sørensen and Lundegaard (2004) who interpret the low-temperature Sb_2S_3 as orthorhombic with pronounced multiple-diffraction effects whereas Kuze et al. (2004) indicate a series of phase transformations from Pbnm via $P2_1nm$ to a monoclinic/triclinic modification below 290 K. The acentric group $P2_1nm$ was already suggested by McKee and McMulan (1975), among others. The two more recent works also contain an exhaustive list of references on this problem. Structures of different members of the $(Bi,Sb)_2S_3$ solid solution series at ambient conditions were published by Kyono and Kimata (2004).

High-pressure study of Sb_2S_3 to 10 GPa was a subject of publication by Lundegaard (2003) (referred to as [1] in the rest of the paper); the analogous study of Bi_2S_3 is the subject of the present contribution.

Experimental

A synthetic bismuthinite was used for this study. For structure analyses a series of X-ray intensity data was collected in the pressure range 0–10 GPa using a CCD-equipped Bruker AXS 4-circle diffractometer, and a DXR-6 Diacell diamond-anvil cell (DAC). The data were collected at 298 K using graphite-monochromatized MoKα radiation. One zero-pressure data set with crystal loaded in DAC and seven high-pressure

Electronic Supplementary Material Supplementary material is available for this article at http://dx.doi.org/10.1007/s00269-005-0033-2 and is accessible for authorized users.

L. F. Lundegaard (✉) · E. Makovicky · T. Balic-Zunic
Geological Institute, University of Copenhagen,
Øster Voldgade 10, 1350 Copenhagen K, Denmark
E-mail: lars.lundegaard@ed.ac.uk

T. Boffa-Ballaran
Bayerisches Geoinstitut, Universität Bayreuth,
95440 Bayreuth, Germany

Present address: L. F. Lundegaard
School of Physics and Centre for Science at Extreme Conditions,
University of Edinburgh, Mayfield Road, Edinburgh EH93JZ, UK

data sets were collected. For this experiment a 220 μm hole was drilled into a steel gasket preindented to a thickness of 80 μm. A 1:4 ethanol:methanol mixture was used as hydrostatic pressure medium. Unit-cell parameters of quartz were used for pressure calibration (Angel et al. 1996). The data was integrated with SAINT+, and XPREP (Bruker 2000) was used for numerical face-indexed absorption correction. Beryllium plugs were used in the optical access holes in the beryllium backing plates. It was therefore possible to calculate the X-ray path length through the DAC-components using the setting angles for each reflection, and from that it was simple to correct the intensities for absorption due to the DAC-components. All the structures were refined with anisotropic atomic displacement parameters (ADP) for Bi and isotropic for S, using SHELXL-97 (Sheldrick 1997). The structures were all refined in the *Pnma* space group, indicated by the intensity statistics and systematic extinction, to *R*-values of ≈0.04 (Table 1). No phase transition was detected in the pressure range 0–10 GPa. F_0/F_c tables are deposited.

Results and discussion

Equation of state

The EoS for bismuthinite was determined using the post-integration unit-cell parameters, because, as it is demonstrated below, satisfactory EoS parameters can be obtained this way when using the applied experimental setup where the intensities are collected from a large set of exposures with a very high spatial resolution.

In paper [1] the unit-cell parameters were first determined from a set of at least 20 reflections, the positions of which were determined with the eight positions centring procedure (Angel et al. 1996). Using this procedure the setting angles for an individual reflection are determined with a precision better than 0.01°, therefore resulting in very precise unit-cell parameters. The second set of parameters in [1] was obtained from the centring information for a large number of reflections obtained from the SAINT+ integration and was in excellent agreement with the first high precision unit-cell parameters. The zero-pressure volume, bulk modulus and its pressure derivative determined from fitting a third-order Birch-Murnaghan (BM3) equation of state to the post-integration unit-cell parameters of stibnite were found to be 487.1(6) Å^3, 27.9(10) GPa and 7.5(5), respectively, which is in very good agreement with the values 487.73(6) Å^3, 26.91(14) GPa and 7.9(1) found in [1] using the eight positions centring procedure.

Unit-cell parameters of Bi_2S_3 were found to alter smoothly with pressure. The zero-pressure bulk modulus, and its pressure derivative were determined from fitting a BM3 equation of state (Birch 1947) to the unit-cell volume data. By substituting the cube of the unit-cell edges for the volume in the equation, a BM3 EoS was fitted to the unit-cell edges (Table 2). The zero-pressure "bulk modulus" obtained from fitting is equal to minus one-third of the inverse of the zero-pressure linear

Table 2 Parameters of the BM3 equation of state

BM3	Zero-pressure value	K_0 (GPa)	K'
V	498.4(7) Å^3	36.6(15)	6.4(5)
a	11.282(26) Å	17.8(41)	14.6(36)
b	3.9728(11) Å	80.6(31)	2.5(6)
c	11.131(5) Å	35.0(12)	3.7(3)

Table 1 Experimental data for Bi_2S_3

Pressure (GPa)	0.0001	0.97	2.43	3.53	5.92	7.22	8.30	9.18
Crystal data								
a (Å)	11.269(2)	11.136(3)	10.987(2)	10.907(3)	10.758(2)	10.701(3)	10.659(2)	10.634(2)
b (Å)	3.9717(3)	3.9574(4)	3.9353(3)	3.9191(4)	3.8833(3)	3.8655(4)	3.8525(3)	3.8423(3)
c (Å)	11.129(2)	11.035(2)	10.903(2)	10.822(2)	10.650(2)	10.565(2)	10.510(2)	10.463(2)
V_{uc} (Å^3)	498.08	486.32	471.41	462.58	444.89	437.03	431.56	427.56
ρ (g/cm^3)	6.856	7.022	7.244	7.383	7.676	7.814	7.913	7.987
μ (mm^{-1})	71.63	73.36	75.68	77.13	80.196	81.64	82.67	83.446
Data collection								
# Measured reflec.	1,419	1,440	1,401	1,381	1,315	1,286	1,281	1,263
# Unique reflec.	254	244	237	236	222	214	217	212
# Observed reflec.[a]	214	201	200	202	195	186	187	179
R_{int}	0.0824	0.0944	0.1095	0.0937	0.0865	0.1115	0.0913	0.1144
$2\theta_{max}$(°)	46.48	46.52	46.46	46.48	46.52	46.42	46.46	46.50
Range of *h, k, l*	$-9 \le h \le 10$	$-9 \le h \le 9$	$-9 \le h \le 9$	$-9 \le h \le 9$	$-8 \le h \le 9$	$-8 \le h \le 9$	$-8 \le h \le 9$	$-8 \le h \le 9$
	$-4 \le k \le 4$	$-4 \le k \le 4$	$-4 \le k \le 4$	$-4 \le k \le 4$	$-4 \le k \le 4$	$-4 \le k \le 4$	$-4 \le k \le 4$	$-4 \le k \le 4$
	$-11 \le l \le 11$	$-10 \le l \le 11$	$-10 \le l \le 11$	$-10 \le l \le 11$	$-10 \le l \le 10$	$-10 \le l \le 10$	$-10 \le l \le 10$	$-10 \le l \le 10$
Refinement								
$R1$ ($\|F_0\| > 4\sigma$)	0.0419	0.0422	0.0352	0.0434	0.0429	0.0423	0.0390	0.0395
w$R2$	0.0863	0.1010	0.0771	0.0966	0.0973	0.0871	0.0817	0.0790
GooF	1.145	1.186	1.112	1.204	1.155	1.122	1.148	1.242
# Parameters	23	23	23	23	23	23	23	23

[a]Criterion for observed reflection is $|F_0| > 4\sigma$

compressibility β_0 of the unit-cell axis. The zero pressure compressibility is defined as $\beta_0 = l_0^{-1}(\partial l/\partial P)_{P=0}$ where l_0 is the length of the unit-cell edge at zero pressure. Comparing the values of bismuthinite and stibnite it can be seen that the latter is generally more compressible with the exception of the *b*-axis direction which itself is the least compressible direction in both structures.

The evolution of unit-cell parameters with increasing pressure is shown in Figs. 1 and 2. The crossing of *a* and *c* parameters that was observed in stibnite at 1.12 GPa (Fig. 3 in [1]) is not found in bismuthinite, but there is a minimum difference in these values at approximately 2.5 GPa (Fig. 2). This difference can be understood in connection with relative sizes of the largely non-compressible rods in the structure of these two compounds. The thickness of the rods, expressed by e.g. the shortest Bi2–S1 or Sb2–S1 distances (see Fig. 4, 9) is substantially larger in Bi_2S_3 (2.59 Å) than in Sb_2S_3 (2.45 Å). On the other hand, their extension perpendicular to this direction expressed as the distance between marginal S atoms on the side of the rod, is practically the same: 8.01 Å in Bi_2S_3 and 8.03 Å in Sb_2S_3 (all values refer to room temperature). As seen in Fig. 4, the rods have their extended direction oriented at a low angle to the *c*-axis.

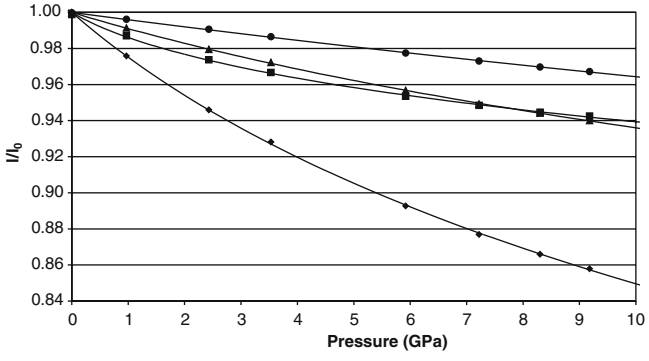

Fig. 1 Evolution of unit-cell parameters of bismuthinite with increasing pressure. Values are given relative to their zero pressure value. *Squares* indicate *a*, *circles b* and *triangles c* value. *Rhombs* stand for unit-cell volume

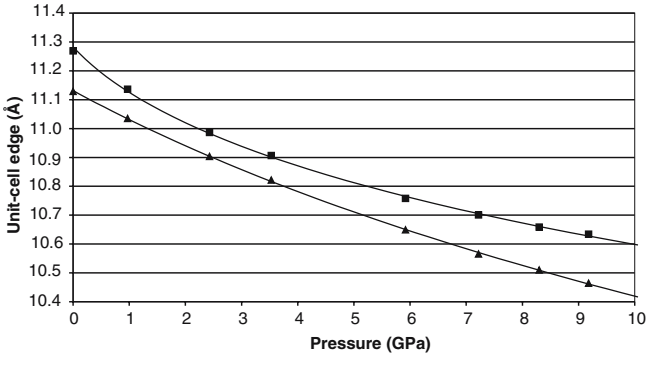

Fig. 2 Observed *a* and *c* unit-cell parameters of bismuthinite. The *lines* are obtained by fitting a BM3 equation of state to the unit-cell parameters. *Squares* indicate *a*, *triangles c* parameter

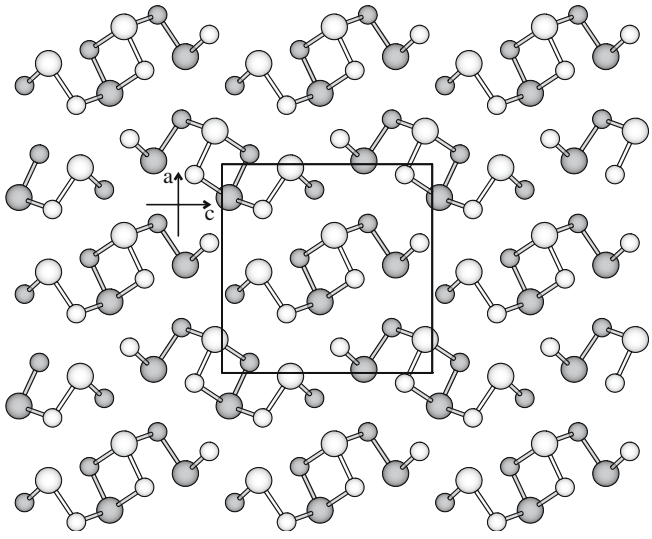

Fig. 3 Structure of bismuthinite in the *Pnma* setting. *Grey circles* represent atoms on the $y = 0.25$ mirror plane, *white circles* represent atoms on the $y = 0.75$ mirror plane. *Large circles* are Bi atoms and *small circles* are S atoms. For atom labels see Fig. 4

The compression of the structure is achieved mostly by a decrease of the inter-rod space. In the first phase of compression this is accompanied by the fastest decrease in the *a*-axis which is longer than the *c*-axis in both compounds at ambient pressure. In stibnite this makes the *a*-axis period shorter than that of the *c*-axis, while in bismuthinite with thicker rods this situation is never achieved. The trend in compressibility along the two axes changes at higher pressures. For stibnite the *a* and *c*-axes stay equal up to 10 GPa, while for bismuthinite after 5 GPa the compressibility along the *c*-axis is even larger than along the *a*-axis.

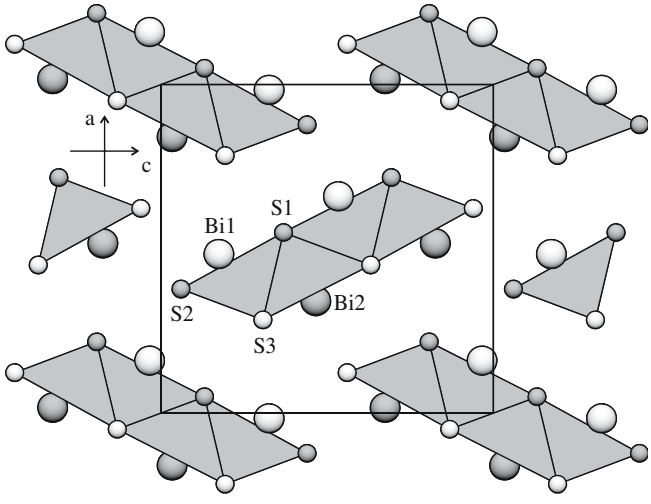

Fig. 4 Grey polyhedra represent the rod volume (V_{rod}) and the rest of the unit-cell volume is defined as the lone electron pair volume (V_{lone}). *Grey circles* represent atoms on the $y = 0.25$ mirror plane, *white circles* represent atoms on the $y = 0.75$ mirror plane. *Large circles* are Bi atoms and *small circles* are S atoms

Structure data

The atom positions of the refined bismuthinite structures are given in Table 3, and the ADP are given in Table 4. Tables with the full anisotropic ADPs are deposited.

As in [1], related sulfides without the lone electron pair will be compared to bismuthinite, in order to gain insight in the pressure effect on the lone electron pair. The related sulfides are Dy_2S_3, and U_2S_3 but also a zero-pressure refinement of Bi_2S_3 has been added to this study (see [1] for references). The values for these three structures have been plotted in a column to the left of the zero-pressure axis to avoid overlap. The convention used is that black points refer to high-pressure bismuthinite data, white points refer to high-pressure stibnite data and grey points are zero-pressure values for Dy_2S_3, Bi_2S_3 and U_2S_3 (In Figs. 5, 6, 7, 8). The effective ionic radii of the trivalent ions Sb^{3+}, Dy^{3+}, Bi^{3+} and U^{3+} are 0.76, 0.91, 1.03 and 1.03 Å, respectively (Shannon 1976).

Principal features

Similar to stibnite, the crystal structure of bismuthinite consists of tightly-bonded rods Bi_4S_6 in a herring-bone arrangement (Fig. 3). All Bi atoms have three short, strong bonds to sulfur, accompanied by two to three longer and weaker bonds, whereas their lone electron pairs are oriented into the inter-rod space. As already ascertained by the structure determinations quoted above, the activity of lone electron pairs in Bi_2S_3 is less pronounced than in Sb_2S_3, with lesser differences between various categories of M–S distances as a consequence.

Unlike stibnite, bismuthinite forms a complete solid solution with $CuPbBiS_3$ and is a parent structure to a series of superstructures resulting from a low-temperature dissociation of the Bi_2S_3–$CuPbBiS_3$ solid solution. It is also related to the homeotypic M_2S_3 sulfides of the elements without a lone electron pair effect—Nd, Dy and U.

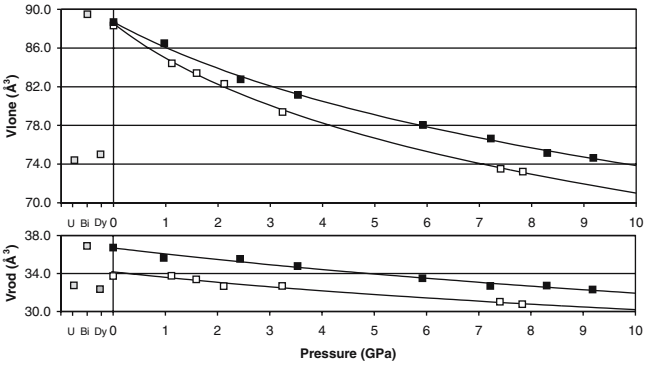

Fig. 5 Calculated inter-rod volume (V_{lone}) and rod volume (V_{rod}). *Black squares* represent the bismuthinite pressure data. *White squares* represent stibnite pressure data, and the *grey squares* represent zero pressure data for Dy_2S_3, Bi_2S_3 and U_2S_3. The curves are obtained by fitting a BM3 equation of state to the volumes

Table 3 Atom positions

Press. (GPa)	0.0001	0.97	2.43	3.53	5.92	7.22	8.30	9.18
Bi1								
x	0.0164(2)	0.0123(2)	0.0077(2)	0.0049(2)	−0.0004(2)	−0.0029(2)	−0.0046(2)	−0.0056(2)
z	0.6745(2)	0.6746(2)	0.6744(1)	0.6744(2)	0.6744(2)	0.6744(2)	0.6746(2)	0.6748(2)
Bi2								
x	0.3406(3)	0.3381(3)	0.3347(2)	0.3331(3)	0.3292(2)	0.3275(2)	0.3263(2)	0.3253(2)
z	0.4661(2)	0.4658(2)	0.4660(1)	0.4663(2)	0.4668(2)	0.4674(1)	0.4674(2)	0.4677(2)
S1								
x	0.0494(16)	0.0503(16)	0.0526(12)	0.0527(15)	0.0523(14)	0.0493(13)	0.0534(14)	0.0529(14)
z	0.1311(11)	0.1266(11)	0.1294(9)	0.1280(11)	0.1297(10)	0.1296(9)	0.1301(10)	0.1296(10)
S2								
x	0.3773(17)	0.3742(16)	0.3744(13)	0.3737(15)	0.3754(13)	0.3745(13)	0.3752(13)	0.3724(13)
z	0.0604(12)	0.0603(12)	0.0591(9)	0.0610(11)	0.0599(10)	0.0607(10)	0.0613(10)	0.0602(11)
S3								
x	0.2165(16)	0.2171(17)	0.2200(12)	0.2211(17)	0.2207(13)	0.2232(14)	0.2225(14)	0.2223(15)
z	0.8069(12)	0.8062(12)	0.8033(9)	0.8026(13)	0.7983(10)	0.7990(10)	0.7966(10)	0.7963(10)

The *y* coordinate is 0.2500(0) for all atom positions in the table

Table 4 Atomic displacement factors

Press. (GPa)		0.0001	0.97	2.43	3.53	5.92	7.22	8.30	9.18
Bi1	U_{eq}	0.0204(10)	0.0192(11)	0.0168(9)	0.0173(11)	0.0161(10)	0.0160(9)	0.0157(9)	0.0155(9)
Bi2	U_{eq}	0.0210(10)	0.0223(11)	0.0200(8)	0.0209(10)	0.0182(10)	0.0177(10)	0.0167(9)	0.0171(10)
S1	U_{iso}	0.019(3)	0.014(3)	0.015(2)	0.012(3)	0.014(3)	0.011(2)	0.012(3)	0.013(3)
S2	U_{iso}	0.022(3)	0.016(3)	0.017(2)	0.014(3)	0.015(3)	0.016(3)	0.014(3)	0.015(3)
S3	U_{iso}	0.019(3)	0.018(3)	0.015(2)	0.021(3)	0.012(3)	0.013(2)	0.015(3)	0.013(3)

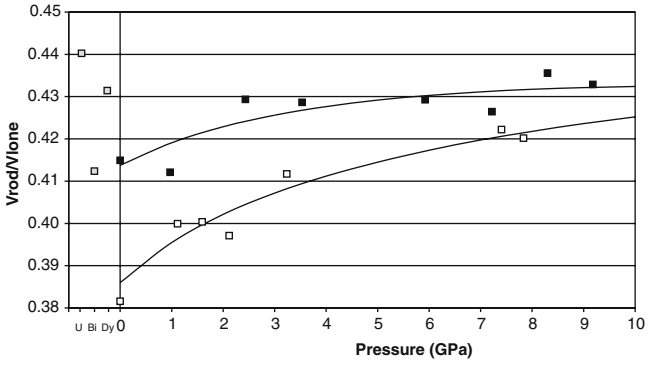

Fig. 6 Observed ratio between the rod volume and the lone electron pair volume. *Black squares* represent the bismuthinite pressure data. *White squares* represent stibnite pressure data, and the *grey squares* represent zero pressure data for Dy_2S_3, Bi_2S_3 and U_2S_3

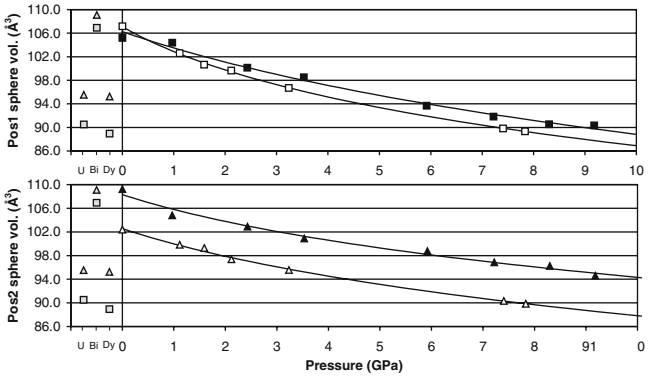

Fig. 7 Fitted sphere volume for the two seven-coordinated cation positions. *Squares* indicate position 1 and *triangles* position 2. *Black symbols* represent the bismuthinite pressure data. *White symbols* represent stibnite pressure data, and the *grey symbols*

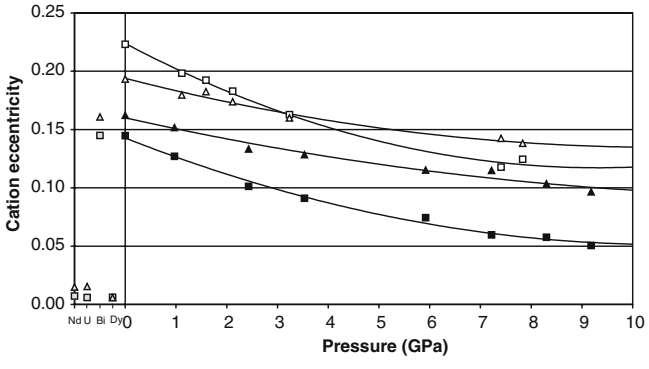

Fig. 8 Cation eccentricities for the two seven-coordinated cation positions. *Squares* indicate position 1 and *triangles* position 2. *Black symbols* represent the bismuthinite pressure data. *White*

Modules

Similar to [1], the crystal structure of bismuthinite has been divided into rod volumes, comprising the four columns of square pyramids in the Bi_4S_6 rods, and the inter-rod volume, defined as the volume influenced by lone electron pairs. This treatment allows us to separate the bulk effects of pressure on these qualitatively different bonding environments. As illustrated in Fig. 4, this division is based on the geometry of anion framework.

Figure 5 illustrates a much larger compressibility of the inter-rod volume compared to the rod volume. The lone-pair compressibility for Sb_2S_3 is initially more pronounced, gaining and maintaining a difference of about 3 $Å^3$ for pressures up to 10 GPa. The rod volume of Sb_2S_3 is smaller by about 3 $Å^3$ already at ambient pressure, and maintains this difference up to and through 10 GPa.

The ratio between the rod volume and the interrod volume changes much more for Sb_2S_3 than for Bi_2S_3 (Fig. 6). The left-hand side of Fig. 6 shows that with rising pressure the ratio in Bi_2S_3 approaches that in U_2S_3 and Dy_2S_3, two compounds without steric lone electron pair activity.

Coordination polyhedra

The two independent Bi positions, Bi1 at the margin of the Bi_4S_6 ribbon and Bi2 placed around the centre of the ribbon, differ in their coordination and pressure behaviour. Both are seven-coordinated but, in relation to the 4 Å axis, Bi1 polyhedron is a monocapped "lying" prism whereas Bi2 a similar "standing" prism. The total volume of a sphere circumscribed to the coordination polyhedron of Bi1 is very close, and develops nearly parallel to, that of Sb1 in stibnite (Fig. 7). However, the values for the no. 2 position are markedly higher for bismuth. The more pronounced compressibility of Sb1 up to about 3.5 GPa is the only important difference between Sb_2S_3 and Bi_2S_3.

The same trend is obvious from the plot of cation eccentricity (Fig. 8) expressed as a fraction of sphere radius (Balic-Zunic and Makovicky 1996). When comparing the Sb and Bi cation eccentricity with those of U and Dy, it is clear that the structure type alone does not force eccentricity upon the cations involved, but it is the lone electron pair of Sb and Bi that generates the eccentricity of cation positions in these sulfides. Cation eccentricity is therefore a very good parameter to quantify the lone electron pair activity. Results show that the compression mechanism in Sb_2S_3 and Bi_2S_3 up to 10 GPa is of the same kind. The stereo-chemical expression decreases, but it is still visible at the highest applied pressures. For Sb it is at all pressures more expressed than for Bi. The examination of trends (see especially Figs. 6, 8) shows that the general structural characteristics of Sb_2S_3 only at 5 GPa resemble

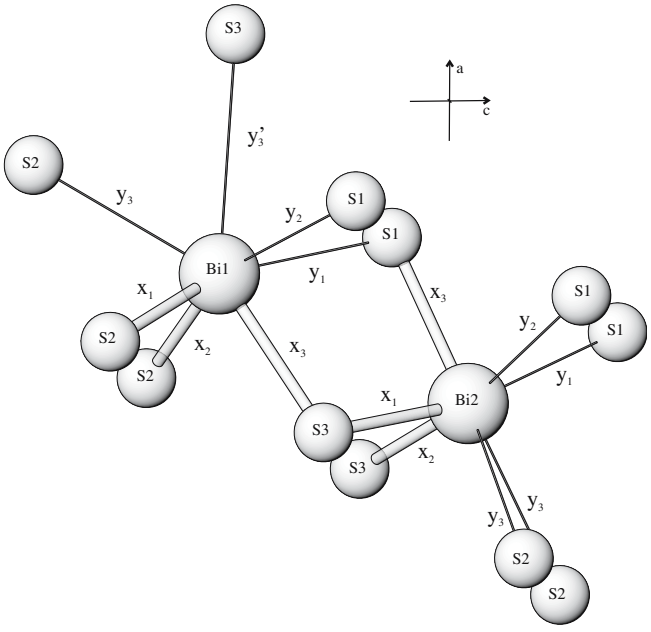

Fig. 9 Bond pairs as defined for the two coordination polyhedra. Bond pairs *y*:*x* are composed of a short *x*-bond and a longer opposing *y*-bond

completely those of Bi_2S_3 at room pressure. Comparison of Figs. 5, 6 and 7 with Fig. 8 suggest that the distortions of the structure motif, introduced by the accommodation of the lone electron pair, are largely eliminated at the pressures where the lone electron pair activity is sufficiently reduced.

Bond lengths

Figures 9, 10, 11 demonstrate the influence of pressure on selected individual Bi–S bonds in the coordination polyhedra of the Bi1 and Bi2 positions and offer a

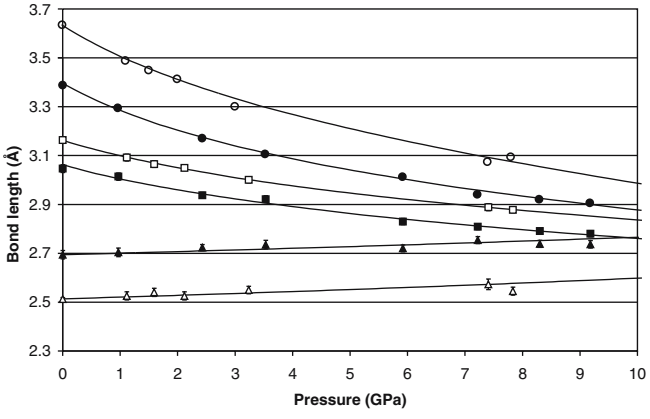

Fig. 10 Plot of the y'_3, y_3 and x_3 bonds for cation position 1. *Black symbols* represent the bismuthinite data and *white symbols* represent stibnite data. *Circles, squares* and *triangles* represent the y'_3, y_3 and x_3 bonds, respectively

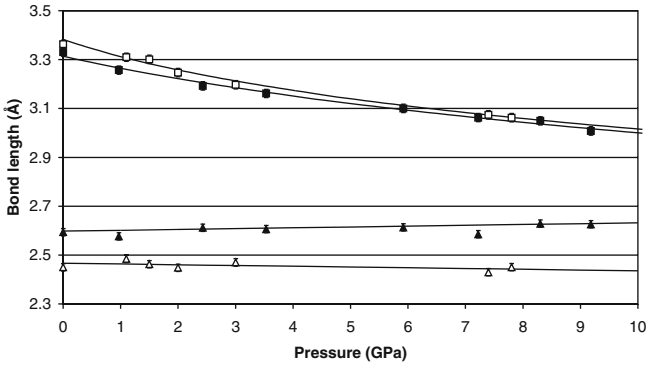

Fig. 11 Plot of the y_3:x_3 bond pair for cation position 2. *Black symbols* represent the bismuthinite data and *white symbols* represent stibnite data. *Squares and triangles* represent the y_3 and x_3 bonds, respectively

comparison with the behaviour of Sb1 and Sb2. The bonds selected are the apical short bonds x_3 of the square coordination pyramids MS_5 and the opposing long distances, below the base of the pyramid, denoted as y_3 (Fig. 9). Both cation positions show a similar trend: as the long y_3 distances show a non-linear decrease with increasing pressure, the short apical x_3 distances show a slight linear increase in the entire range of pressures studied. Corresponding trends in the remaining pairs of opposing bonds in each polyhedron contribute to the trend in eccentricities shown in Fig. 8. Trends observed in Sb_2S_3 are the same, but the

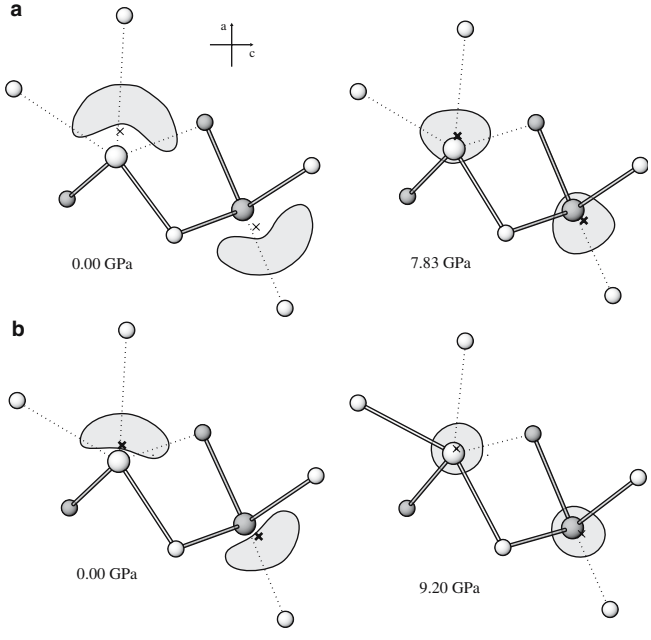

Fig. 12 Schematic model explaining the changes in coordination for Sb atoms in stibnite (**a**) and the changes in coordination for Bi atoms in bismuthinite (**b**). The *cross* marks the position of the centroid calculated using the procedure of Balic-Zunic and Makovicky (1996). For atom labels, see Fig. 9

difference in bond lengths of the x_3 and y_3 bonds/distances is more pronounced. Thus, the equalisation of the x_3 and y_3 bond length for Bi1 at about 10 GPa will occur for Sb1 at much higher pressures, if at all. The additional, longest Bi1–S3 distance (y'_3) is nearly parallel to the initially 'softest' [100] direction. It is the fastest decreasing distance in the M_2S_3 structure when pressure increases. The y'_3:x_3 trend copies in principle the y_3:x_3 trend for Bi1 but with a double decrease in the y'_3 distance. The equalisation of the x_3 and y'_3 distances can be predicted at about 13 GPa.

Lone electron pairs

The seemingly contradictory behaviour of short M–S bonds with pressure is typical for the lone electron pair elements As, Sb and Bi. Berlepsch et al. (2001) demonstrated the hyperbolic interdependence of the opposing bond lengths in the coordination polyhedra of these M^{3+} cations. Increase in the long M–S distance leads to the decrease in the opposing bond length along a hyperbolic trajectory in the plot of opposing bond distances, and vice versa. This is obviously true also for the case of increasing pressure although the hyperbolic trend at any pressure differs from that at ambient conditions (Lundegaard 2003).

A qualitative explanation of this effect is illustrated in Fig. 12. The customary shape of the volume occupied by the lone electron pair is shaded in this picture and the centroid of the relevant coordination polyhedron is indicated by a cross. Assignment of the lone electron pair volumes is supported by semiquantitative calculations using the ABINIT package (Gonze et al. 2002) based on density functional theory using pseudopotentials and a plane wave basis (Lundegaard 2003). The very asymmetric configuration in Sb_2S_3 and Bi_2S_3 at ambient conditions (for differences see Fig. 12) becomes much more symmetric at high pressure, with the centroids approaching closely the cation sites. By implication, the loci of the lone electron pair in the coordination polyhedra follow, enveloping partly the cations. Thus, their repulsive action on the S atoms situated at the long M–S distances decreases, whereas their influence on the S atoms which are tightly bonded to M, increases.

Acknowledgements This research is part of the project no. 57252 of the Danish State Research Council.

References

Łukaszewicz K, Pietraszko A, Stepień-Damm J, Grigas J, Kajokas A (1997) Crystal structure of stibnite Sb_2S_3 in phase II at 320 K. Polish J Chem 71:390–395

Ščavničar S (1960) The crystal structure of stibnite: a redetermination of atomic positions. Z Kristallogr 114:86–97

Angel R, Allen DR, Miletich R, Finger LW (1996) The use of quartz as an internal pressure standard in high-pressure crystallography. J Appl Crystallogr 30:461–466

Balic-Zunic T, Makovicky E (1996) Determination of the centroid or 'the best centre' of a coordination polyhedron. Acta Crystallogr B52:78–81

Bayliss P, Nowacki W (1972) Refinement of the crystal structure of stibnite, Sb_2S_3. Z Kristallogr 135:308–315

Berlepsch P, Makovicky E, Balic-Zunic T (2001) Crystal chemistry of meneghinite homologues and related sulfosalts. N Jb Miner Mh 3:115–135

Birch F (1947) Finite elastic strain of cubic crystals. Phys Rev 71:809–824

Bruker (2000) SMART, SAINT + and XPREP. Bruker AXS Inc., Madison

Gonze X, Beuken J-M, Caracas R, Detraux F, Fuchs M (2002) First-principles computation of material properties: the ABINIT software project. Comput Mater Sci 25:478–492

Hofmann W (1933) Die Struktur der Minerale der Antimonitgruppe. Z Kristallogr 86:225–245

Kupčik V, Veselá-Nováková L (1970) Zur Kristallstruktur des Bismuthinits, Bi_2S_3. Tschermaks Mineralogische Petrographische Mitteilunge 14:55–59

Kuze S, Boulay D, Ishizawa N, Saiki A, Pring A (2004) X-ray diffraction evidence for a monocline form of stibnite, Sb_2S_3, below 290 K. Am Mineral 89:1022–1025

Kyono A, Kimata M (2004) Structural variations induced by difference of the inert pair effect in the stibnite–bismuthinite solid solution series $(Sb,Bi)_2S_3$. Am Mineral 89:932–940

Kyono A, Kimata M, Matsuhisa M, Miyashita Y, Okamoto K (2002) Low-temperature crystal structure of stibnite implying orbital overlap of Sb 5s(2) inert pair electrons. Phys Chem Miner 29(4):254–260

Lundegaard LF (2003) A structural study of Sb_2S_3 and Bi_2S_3 at non-ambient conditions. Cand Scient Thesis, Geological cInstitute, University of Copenhagen

Lundegaard LF, Miletich R, Balic-Zunic T, Makovicky E (2003) Equation of state and crystal structure of Sb_2S_3 between 0 and 10 Gpa. Phys Chem Miner 30(8):463–468

McKee DO, McMulan JT (1975) Comment on the structure of antimony trisulfide. Z Kristallogr 142:447–449

Rinkevichius VS, Mikalkevichius MP (1967) Pyroelectric effect in antimony trisulfide single crystals. Sov Phys Solid State USSR 9(10):2360

Shannon RD (1976) Revised effective ionic radii and systematic studies of interatomic distances in halides and chalcogenides. Acta Crystallogr A32:751–767

Sheldrick GM (1997) Shelxl-97 program for refinement of crystal-structures. University of Göttingen

Sørensen HO, Lundegaard LF (2004) On the space-group dispute of stibnite. J Appl Crystallogr 37:156–158